Research Article

Muhammad Ramzan*, Yazeed Alkhrijah, Saeed Abbas, Nazia Shahmir, Ibtehal Alazman, and Wei Sin Koh

Comparative reaction dynamics in rotating nanofluid systems: Quartic and cubic kinetics under MHD influence

https://doi.org/10.1515/phys-2025-0222
received March 19, 2025; accepted September 29, 2025

Abstract: An electrically conducting Reiner–Rivlin nanoliquid flow is considered over a rough, infinitely spinning disk based on a von Kármán model. The flow incorporates partial slip conditions and a temperature jump at the disk surface. This investigation seeks to establish a more precise and practical framework for advanced thermal-fluid systems, with specific relevance to microscale heat management and electrohydrodynamic technologies. The novelty lies in addressing the comparative appraisal of quartic and cubic chemical reactions as these possess pivotal applications, including advanced cooling systems, corrosion and material processing, electromagnetic and MHD applications, and aerospace and turbomachinery. Additionally, Brownian motion and thermophoresis effects are included owing to nanoparticles. The 3-stage Lobatto IIIa method of MATLAB software is applied to compute the numerical solution of the present model. Results are demonstrated in the form of illustrations and tables. The velocity and temperature profiles display contrasting trends for the slip parameter. The fluid concentration decreases with the Reiner–Rivlin parameter and the Schmidt number. In addition, the heat flux rate is higher for a quartic chemical reaction than for a cubic chemical reaction. This study can be applied to microfluidic devices, rotary heat exchangers, and rotating machinery in aerospace and biomedical systems, where enhanced heat transfer, complex fluid behavior, and realistic boundary effects like slip, roughness, and magnetic fields are critical. A validation of the presented data is also a part of this study. To draw the graphs and for the tabulated values, the assumed ranges of the involved parameters are as follows:

$$2 \le \mathrm{Pr} \le 20,\quad 0.1 \le \gamma \le 0.5,\quad 5 \le M \le 15,\quad 0.2 \le \alpha \le 0.6,$$
$$4 \le N_{\mathrm{b}} \le 6,\quad 0.1 \le N_{\mathrm{t}} \le 0.3,\quad 0.3 \le K \le 0.4,\quad 2.5 \le Sc \le 3.5.$$

Keywords: quartic and cubic chemical reactions, Reiner, Rivlin nanofluid, energy efficiency, magnetic field, rotating disk

Nomenclature

u, v, w	velocity components (m/s)
T	temperature profile (K)
T_{w}	temperature of the fluid near a disk (K)
η	similarity variable
T_∞	ambient fluid temperature (K)
ρ_{f}	density of fluid (kg/m^3)
Pr	Prandtl number
D_{T}	thermophoretic diffusion coefficient
$D_{\mathrm{A}}, D_{\mathrm{B}}$	Brownian diffusion coefficients
N_{t}	thermophoresis parameter
L_1	wall slip coefficient
Ω	rotating parameter (1/s)
K_1	homogeneous reaction strength
B_0	magnetic flux
N_{b}	Brownian motion parameter
Nu	Nusselt number
K	Reiner–Rivlin parameter
p	Pressure

*** Corresponding author: Muhammad Ramzan,** Department of Mathematics and Statistics, College of Science, Imam Mohammad Ibn Saud Islamic University (IMSIU), Riyadh 13318, Saudi Arabia, e-mail: mramzan@bahria.edu.pk
Yazeed Alkhrijah: Department of Electrical Engineering, College of Engineering, Imam Mohammad Ibn Saud Islamic University (IMSIU), Riyadh, 13318, Saudi Arabia
Saeed Abbas, Nazia Shahmir: Department of Computer Science, Bahria University, Islamabad, 44000, Pakistan
Ibtehal Alazman: Department of Mathematics and Statistics, College of Science, Imam Mohammad Ibn Saud Islamic University (IMSIU), Riyadh, 13318, Saudi Arabia
Wei Sin Koh: Faculty of Business and Communications, INTI International University, Putra Nilai, Nilai, Negeri Sembilan, 71800, Malaysia

Re	Reynolds number
σ_f	electrical conductivity
k_f	thermal conductivity (W/mK)
a, b	chemical species
Sc	Schmidt number
τ	heat capacity relationship
L_3	temperature slip coefficient
a, b	chemical reaction parameters
K_2	heterogeneous reaction strength
r, ϕ, z	axis

1 Introduction

Visco-inelastic/elastic liquids, polar liquids, anisotropic liquids, and liquids with microstructures are the main classifications for non-Newtonian liquid models. One significant type of non-Newtonian liquid is the Reiner–Rivlin liquid flow model. The idea of the Reiner–Rivlin model was pitched by Reiner [1] and Rivlin [2], which can predict both elasticity and viscosity, making them suitable for accurate flow control and shear constraints. This model is equally useful in predicting the flow trend of biological and geological materials, along with food products and polymers. Researchers are still looking for new avenues in varied scenarios, considering the Reiner–Rivlin fluid model. Sabu *et al.* [3] examined the nanoparticle volume fraction and thermal fields increase in response to the Reiner–Rivlin liquid's characteristics, attributed to enhanced non-Newtonian behavior resulting from improved cross-viscosity. The heat transfer behavior of the Reiner–Rivlin fluid with Stefan blowing effects on a radially stretched disk is investigated by Kumar and Sharma [4]. They discovered that raising the Reiner–Rivlin and stretch strength parameters affects the radial and rotational velocities. The Reiner–Rivlin nanoliquid flow over a stretchable rotating disk problem was solved using the numerical and homotopy analysis method (HAM) by Nebiyal *et al.* [5]. The outcome depicts that the HAM and numerical solution have similar results. The study also showed that the Schmidt number plays a crucial role in influencing the system's entropy rate. Faisal *et al.* [6] developed a mathematical model for the Reiner–Rivlin liquid flow between two rotating stretchy disks, incorporating Cattaneo–Christov heat transmission. Using the HAM and numerical solution, they observed that lower temperatures occur at the top and bottom surfaces of the disks in their stationary positions. Additionally, it was observed that the fluid temperature decreases with increasing Cattaneo–Christov parameter values. A mathematical equation for the flow of a Reiner–Rivlin nanoliquid around an isothermal sphere containing a suspension of microorganisms is introduced by Alarabi *et al.* [7]. The analysis is assisted by a magnetic field and a zero-mass flux constraint at the surface. The results indicate that the dimensionless velocity at the surface declines with increasing values of the Brownian motion parameter. Cham *et al.* [8] considered viscous dissipation and investigated heat and mass transfer in the Reiner–Rivlin flow on a horizontal stretched cylinder. The Soret effect, reaction rate, magnetic impact, and entropy creation rate are examined as key elements. Muhammad *et al.* [9] studied how a magnetic field affects a Reiner–Rivlin nanofluid flow when it is time-dependent. More studies on the Reiner–Rivlin nanofluid flow may be found in the literature [10–12].

The exploration of cubic chemical reactions in fluid mechanics has many useful applications. These reactions, which depend on the cube of the reactant concentration, are important in autocatalysis, chemical engineering (such as combustion analysis and reactor design), environmental science (including air pollution control and atmospheric chemistry), and biology (such as drug delivery and enzyme activity). The interaction between these reactions and fluid flow is crucial in both smooth and turbulent flows, where mixing and reaction rates can have a major impact on system efficiency. Despite the difficulties of adequately modeling these nonlinear systems, combining cubic chemical reactions with fluid mechanics gives important insights for expanding technology in energy, the environment, biomedical engineering, and industrial processes. Researchers keenly observed numerous fluid flow scenarios considering chemical reactions. Ramzan *et al.* [13] determined the role of an autocatalytic chemical reaction and inertial drag in the Ostwald–de Waele nanoliquid flow along a rotating disk with a non-uniform heat source sink. It is claimed that the reaction is triggered more effectively by surface catalysis. The role of cubic autocatalytic chemical reactions in the magnetic Prandtl nanoliquid flow due to an extending surface with entropy analysis is numerically scrutinized by ur Rahman *et al.* [14]. The results indicated that higher estimations of the magnetic factor led to significant entropy production. Xin *et al.* [15] numerically computed the flow of a radiative Carreau nanoliquid under the consequences of cubic autocatalysis, inclined magnetic flux, and temperature-dependent thermal conductivity along a bidirectional stretching geometry. Outcomes determined that the temperature of the fluid is more pronounced for a greater radiation factor. Recently, the ferromagnetic non-Newtonian liquid flow under the influence of the modified Fourier law, magnetic dipole, and cubic autocatalysis chemical reaction was scrutinized by Khan *et al.* [16].

The study of quartic chemical reactions examines how fluids move and react when the reaction rate depends on

the fourth power of the reaction concentration. Quartic reactions play a key role in systems with complex reaction processes, such as certain polymerizations, catalytic cycles, and metabolic pathways. Understanding these reactions helps in designing advanced reactors, improving production efficiency, and predicting system behavior under different flow conditions. In environmental science, they are used to studying atmospheric reactions and modeling oxidation processes for breaking down pollutants. Atif *et al.* [17] assessed the flow of radiative tangent hyperbolic nanoliquid with the influences of quartic chemical reaction along a paraboloid geometry with buoyancy force. An important outcome revealed that the heat transmission rate declined for higher values of the velocity power index factor. The consequences of the homogeneous–heterogeneous quartic autocatalytic reaction on the viscous fluid flow over the exterior of a rotating cylinder were discussed by Saranya *et al.* [18]. The findings showed that increasing the intensity of the magnetic fields enriched the heterogeneous reaction at the surface. Next, Oreyeni *et al.* [19] comprehended the consequences of the quartic autocatalytic chemical reaction over the electromagnetic Casson liquid flow over a stratified surface of variable thickness. The flow of the magnetized hybrid nanoliquid under the effects of the quartic autocatalytic chemical reaction, Joule heating, and inertial drag force was examined by Riaz *et al.* [20]. The surface drag coefficient increases along the axial direction by increasing the inertial parameter. Mehmood *et al.* [21] examined the role of quartic autocatalytic reactions and activation energy over the Maxwell nanoliquid flow over an extending geometry with the Thompson and Trion slip. The results revealed that the velocity ratio factor and thermal expansion had contrasting significance on the heat transmission rate. More work on chemical reactions may be found in previous work [11,22].

In all the above-cited works, either quartic or cubic chemical reactions are deliberated separately. However, no existing studies have conducted a comparative analysis of quartic and cubic chemical reactions affecting the flow of the Reiner–Rivlin nanoliquid over a disk subjected to an external magnetic field. The above flow is assisted by the partial slip and the temperature jump conditions. The bvp4c method in MATLAB is employed to develop a mathematical solution. Furthermore, the results are thoroughly explained through illustrations and tabulated values.

The core purposes of the anticipated model are the following:

- To determine the behavior of the velocity and temperature profiles against the partial slip parameter.
- To gauge the impact of the magnetic field on the velocity profiles.
- To observe the role of strong magnetic flux in the disk's continuous spin.
- To determine the consequences of the thermal slip parameter on the temperature distribution in both cases of chemical reactions.
- To assess the impact of the Reiner–Rivlin parameter on the concentration profile in the cases of cubic and quartic chemical reactions.
- To gauge the impact on the heat flux rate while comparing quartic and cubic chemical reactions.

2 Mathematical formulation

The anticipated model is based on the following assumptions:

- Consider a laminar, unsteady state flow of the Riner–Rivlin nanofluid in contact with a rotating disk at constant angular velocity (Ω). The constitutive equation for the Reiner–Rivlin fluid is

$$\tau = \mu A_1 + \alpha_1 A_2, \tag{1}$$

  where τ is the Cauchy stress tensor, μ is the dynamic viscosity, α_1 is the material parameter (the Reiner–Rivlin parameter), A_1 is the first Rivlin–Ericksen tensor (rate of strain), and A_2 is the second Rivlin–Ericksen tensor. Depending on the value of α_1, the fluid may exhibit nonlinear viscosity, *i.e.*, the viscosity increases or decreases with the shear rate. Adding nanoparticles to a Reiner–Rivlin fluid enhances its thermal conductivity and alters its viscosity, leading to improved heat transfer but a more complex flow behavior. These changes introduce additional effects like Brownian motion and thermophoresis, making the mathematical model highly nonlinear and suitable for advanced thermal applications.
- The effects of thermophoresis and Brownian motion are incorporated into chemical reactions.
- A uniformly strong magnetic flux (B_0) is applied along the axial direction.
- It is believed that the magnetic Reynolds number is small enough to produce a minimally induced magnetic field.
- The temperature and concentration at the free stream are denoted by T_∞ and C_∞.
- The anticipated model is assisted by the partial slip and temperature jump conditions.
- The concentration distribution is assisted by homogeneous–heterogeneous conditions.
- The whole scenario is depicted in Figure 1.

The predicted model is governed by the following partial differential equations [17,23,24]:

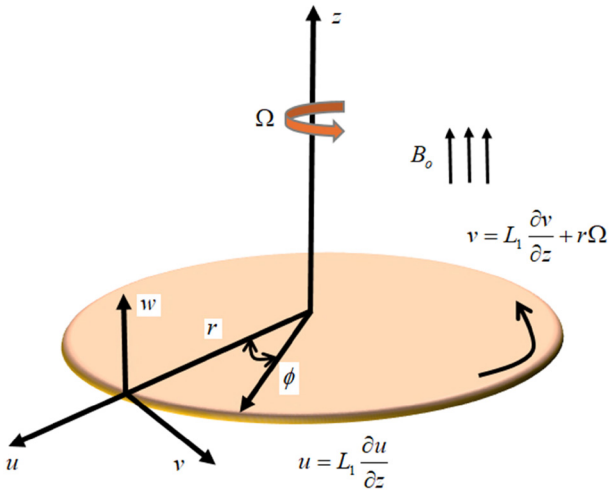

Figure 1: Flow geometry.

$$\frac{\partial u}{\partial r} + \frac{u}{r} + \frac{\partial w}{\partial z} = 0, \tag{2}$$

$$\rho_f\left(u\frac{\partial u}{\partial r} + w\frac{\partial u}{\partial z} - \frac{v^2}{r}\right) = \frac{\partial \tau_{rr}}{\partial r} + \frac{\partial \tau_{rz}}{\partial z} + \frac{\partial \tau_{rr} - \partial \tau_{rr}}{r} - \sigma_f B_0^2 u, \tag{3}$$

$$\rho_f\left(u\frac{\partial v}{\partial r} + w\frac{\partial v}{\partial z} + \frac{uv}{r}\right) = \frac{1}{r^2}\frac{\partial (r^2\tau_{r\phi})}{\partial r} + \frac{\partial \tau_{z\phi}}{\partial z} + \frac{\partial \tau_{r\phi} - \partial \tau_{\phi r}}{r} - \sigma_f B_0^2 v, \tag{4}$$

$$u\frac{\partial T}{\partial r} + w\frac{\partial T}{\partial z} = \alpha_f\left(\frac{\partial^2 T}{\partial r^2} + \frac{1}{r}\frac{\partial T}{\partial r} + \frac{\partial^2 T}{\partial z^2}\right) + \tau\left[D_B\left(\frac{\partial T}{\partial r}\frac{\partial a}{\partial r} + \frac{\partial T}{\partial z}\frac{\partial a}{\partial z}\right) + \frac{D_T}{T_\infty}\left(\left(\frac{\partial T}{\partial r}\right)^2 + \left(\frac{\partial T}{\partial z}\right)^2\right)\right], \tag{5}$$

where the expressions for the tensor in Eqs. (2) and (3) are formulated as follows:

$$\begin{aligned}
\tau_{rr} &= -p + 2\mu_f u_r + \mu_c[4(u_r)^2 + (u_z + w_r)^2 + (v_r - v/r)^2],\\
\tau_{rz} &= \mu_f(u_z + w_r) + \mu_c[(2u_r)(u_z + w_r) + v_r(v_r - v/r) + 2w_z(u_z + w_r)],\\
\tau_{\phi\phi} &= -p + \mu_f\left(2\frac{u}{r}\right) + \mu_c\left[4(v_z)^2\left(\frac{u}{r}\right)^2 + (v_r - v/r)^2\right],\\
\tau_{r\phi} &= \mu_f(v_r - v/r) + \mu_c\left[(2u_r)(v_r - v/r) + \left(\frac{u}{r}\right)2(v_r - v/r) + 2v_z(u_z + w_r)\right],\\
\tau_{z\phi} &= \mu_f(v_z) + \mu_c\left[(u_z + w_r)(v_r - v/r) + \left(\frac{u}{r}\right)2v_z + 2v_z w_z\right].
\end{aligned} \tag{6}$$

The concentration equation with a cubic chemical reaction is given by [23]

$$u\frac{\partial a}{\partial r} + w\frac{\partial a}{\partial z} = D_A\left(\frac{\partial^2 a}{\partial z^2}\right) - k_1 ab^2 + \frac{D_T}{T_\infty}\left(\frac{\partial^2 T}{\partial z^2}\right), \tag{7}$$

$$u\frac{\partial b}{\partial r} + w\frac{\partial b}{\partial z} = D_B\left(\frac{\partial^2 b}{\partial z^2}\right) + k_1 ab^2 + \frac{D_T}{T_\infty}\left(\frac{\partial^2 T}{\partial z^2}\right), \tag{8}$$

and the concentration equation with a quartic chemical reaction is given by [17]

$$u\frac{\partial a}{\partial r} + w\frac{\partial a}{\partial z} = D_A\left(\frac{\partial^2 a}{\partial z^2}\right) - k_1 ab^3 + \frac{D_T}{T_\infty}\left(\frac{\partial^2 T}{\partial z^2}\right), \tag{9}$$

$$u\frac{\partial b}{\partial r} + w\frac{\partial b}{\partial z} = D_B\left(\frac{\partial^2 b}{\partial z^2}\right) + k_1 ab^3 + \frac{D_T}{T_\infty}\left(\frac{\partial^2 T}{\partial z^2}\right), \tag{10}$$

with wall assumptions [25]:

$$\begin{aligned}
&z = 0 : u = L_1\frac{\partial u}{\partial z}, \quad v = L_1\frac{\partial v}{\partial z} + r\Omega, \quad w = 0,\\
&T = T_w + L_3\frac{\partial T}{\partial z}, \quad D_A\frac{\partial a}{\partial z} = -D_B\frac{\partial b}{\partial z} = k_2 a,\\
&z \to \infty : u \to 0, \quad T \to T_\infty, \quad p \to p_\infty, \quad a \to a_\infty,\\
&b \to 0.
\end{aligned} \tag{11}$$

The following similarity transformations are used to convert the given system into a coupled, dimensionless system of differential equations [23]:

$$\begin{aligned}
&\eta = \sqrt{\frac{\Omega}{\upsilon_f}}z, (u, v, w) = (r\Omega f'(\eta),\\
&r\Omega g(\eta), \ -2\sqrt{\upsilon_f\Omega}f(\eta)),\\
&T = T_\infty + (T_w - T_\infty)\theta(\eta), \ p = p_\infty - \Omega\mu_f P(\eta),\\
&a = a_\infty\phi_1, \ b = a_\infty\phi_2.
\end{aligned} \tag{12}$$

The continuity is identically satisfied, and Eqs. (3)–(11) yield the following:

$$f''' - Mf' + 2ff''g^2 - f'^2 + K(f''^2 + 2f'f''' + g'^2) = 0, \tag{13}$$

$$g'' - 2f'g + 2fg' - Mg - 2K(f'g'' - f''g') = 0, \tag{14}$$

$$\frac{1}{\mathrm{Pr}}\theta'' + f\theta' + N_b\theta'\phi_1' + N_t\theta'^2 = 0. \tag{15}$$

The detailed calculation is given in the Appendix. As discussed by Chaudhary and Merkin [26], both diffusion coefficients are equal, *i.e.*, $D_A = D_B$, indicating that they are of comparable sizes; thus, these coefficients are assumed to be equal by considering $\delta = 1$. Hence, $\phi_1 + \phi_2 = 1$, which will give Eqs. (15) and (16) as follows.

The concentration equation with a cubic chemical reaction is given by

$$\phi_1'' + \mathrm{Sc} f \phi_1' - \frac{1}{2}\mathrm{Sc} K_1 \phi_1 (1 - \phi_1)^2 + \frac{N_t}{N_b}\theta'' = 0, \quad (16)$$

and the concentration equation with a quartic chemical reaction is given by

$$\phi_1'' + \mathrm{Sc} f \phi_1' - \frac{1}{2}\mathrm{Sc} K_1 \phi_1 (1 - \phi_1)^3 + \frac{N_t}{N_b}\theta'' = 0. \quad (17)$$

With transformed constraints at the surface and the boundary [23]:

$$\begin{aligned} &\eta = 0 : f = 0, \ \ f' = \gamma f'', \ \ g = 1 + \gamma g', \ \ \theta = 1 + \alpha\theta', \\ &\phi_1' = K_2 \phi_1, \\ &f' \to 0, \ \ g \to 0, \ \ \theta \to 0, \ \ \phi_1 \to 1, \ \text{as} \ \eta \to \infty. \end{aligned} \quad (18)$$

The parameters in the above system are

$$\begin{aligned} &M = \frac{\sigma_f B_0^2}{\rho_f \Omega}, \quad \mathrm{Pr} = \frac{\upsilon_f}{\alpha_f}, \quad K = \frac{\mu_c \Omega}{\mu_f}, \quad \gamma = L_1\sqrt{\frac{\Omega}{\upsilon_f}}, \\ &\alpha = L_3\sqrt{\frac{\Omega}{\upsilon_f}}, \quad K_1 = \frac{k_1 a_\infty^n}{\Omega}, \quad K_2 = \frac{k_2}{D_A}\sqrt{\frac{\upsilon}{\Omega}}, \\ &\mathrm{Sc} = \frac{\upsilon}{D_A}, \quad N_b = \frac{\tau D_B a_\infty}{\upsilon_f}, \quad N_t = \frac{\tau D_T (T_w - T_\infty)}{\upsilon_f T_\infty}, \\ &\frac{N_t}{N_b} = \frac{D_T (T_w - T_\infty)}{D_B T_\infty a_\infty}, \end{aligned} \quad (19)$$

where M is the magnetic field number, Pr is the Prandtl number, K is the fluid parameter, γ is the velocity slip parameter, L_1 is the wall slip coefficient, α is the thermal slip parameter, K_1 illustrates the homogeneous reaction strength, K_2 depicts the heterogeneous reaction strength, Sc is the Schmidt number, N_b and N_t illustrate the Brownian and thermophoretic parameters, and D_B and D_T are the Brownian diffusion coefficient and thermophoretic diffusion coefficient.

3 Engineering quantities

To determine the local Nusselt number [23], heat flux is calculated as the combined contribution of the conductive heat flux and the heat flux resulting from nanoparticle diffusion:

$$\mathrm{Nu}_r = \frac{rq''}{k(T_w - T_\infty)}, \quad (20)$$

where $q'' = -k\frac{\partial T}{\partial z_{z=0}}$ is the heat flux at the disk.

The following are the dimensionless engineering quantities of interest:

$$\mathrm{Nu}_r \, \mathrm{Re}^{-1/2} = -\theta'(0), \quad (21)$$

where Eq. (21) is a dimensionless expression for the local Nusselt number. However, $\mathrm{Re} = \frac{\Omega r^2}{\upsilon}$ is the local Reynolds number.

4 Numerical solution and tabular results

The problems of fluid flows are handled using varied techniques [27–29]. However, here, the bvp4c, a numerical technique, is engaged; the system of ODEs, along with boundary

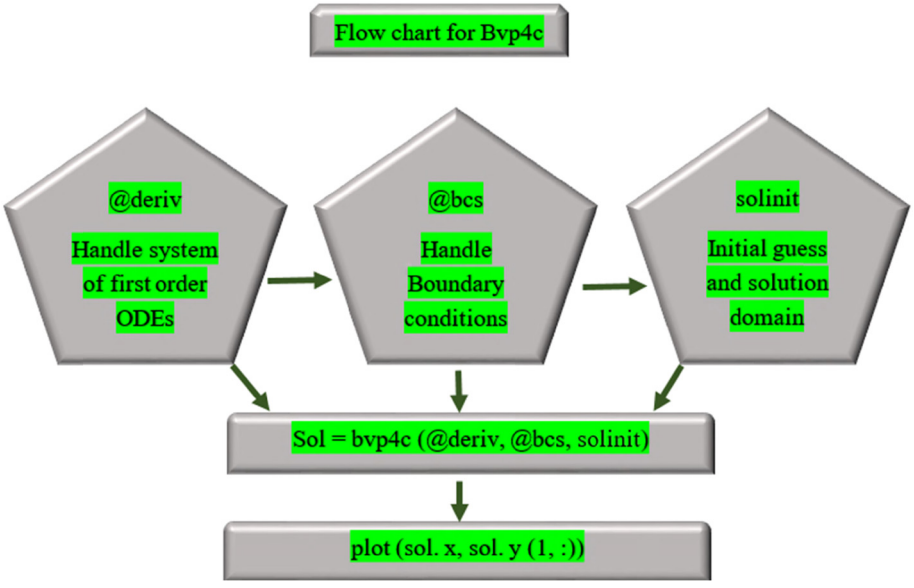

Figure 2: A flowchart of the numerical technique.

Table 1: Validation of the current work with research by Tabassum and Mustafa [30] in a limiting case

K	Tabassum and Mustafa [30]	Present
0	−0.533151	−0.533152
2	−0.453112	−0.453113
4	−0.370251	−0.370252

constraints, is coded in MATLAB. With a tolerance of 10^{-6}, the grid size of 0.01 is considered, and the numerical values produced are valid to the fourth order. The bvp4c algorithm requires that we transform our system into a first-order ODE system. For more information, the flow chart of the numerical technique is shown in Figure 2.

The results of validation and engineering quantities are presented in Tables 1 and 2, respectively. From Table 1, an excellent agreement can be observed from the work of Tabassum and Mustafa [30].

The Nusselt numbers for the cubic chemical reaction and quartic chemical reaction are displayed in Table 2. Except for the Prandtl number, which exhibits increasing behavior, it is observed that the quantity exhibits growing behavior for the thermophoresis parameter N_t, Prandtl number Pr, and Brownian motion parameter N_b in cubic and quartic chemical reactions.

5 Graphical results and discussion

This section provides a thorough overview of the influence of the arising parameters on the associated profiles.

Table 2: Numerical estimates of the local Nusselt number $-\mathrm{Nu_s Re_s}^{-\frac{1}{2}}$ against different parameters

Pr	Nt	α	Nb	$\mathrm{Nu_s Re_s}^{-\frac{1}{2}}$ (cubic chemical reaction)	$\mathrm{Nu_s Re_s}^{-\frac{1}{2}}$ (quartic chemical reaction)
2.0	0.1	0.2	2.0	0.172518	0.265754
3.0				0.188839	0.333443
4.0				0.200340	0.393675
5.0				0.208892	0.448679
	0.2			0.162434	0.596802
	0.3			0.117169	0.529887
	0.4			0.086876	0.478980
		0.3		0.226834	0.643280
		0.4		0.223475	0.608637
		0.5		0.220154	0.577120
			2.1	0.235280	0.706885
			2.2	0.240269	0.732132
			2.3	0.245201	0.757172

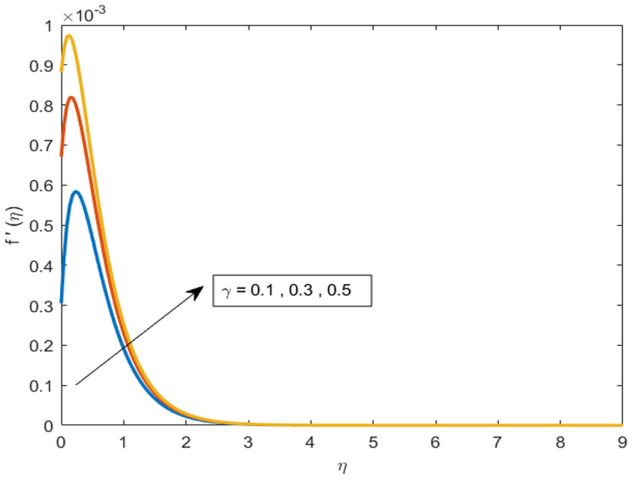

Figure 3: Velocity distribution for the velocity slip parameter γ.

5.1 Velocity radial and axial profiles

Figures 3–5 display the graphs of the radial velocity profile for the velocity slip parameter γ, and the radial and axial velocity distributions for the magnetic parameter M, respectively.

Figure 3 displays the velocity distribution in relation to the various values of the velocity slip parameter γ. It was observed that the velocity profile displayed increasing behavior as the velocity slip parameter (γ) increased, as the slip parameter allowed the liquid to move faster in the vicinity of the surface. In the case of a no-slip condition, the fluid remains stagnant at the boundary. With the inclusion of the slip condition, the fluid velocity at the boundary becomes non-zero, which reduces the shear resistance and enhances the overall flow velocity. As the slip

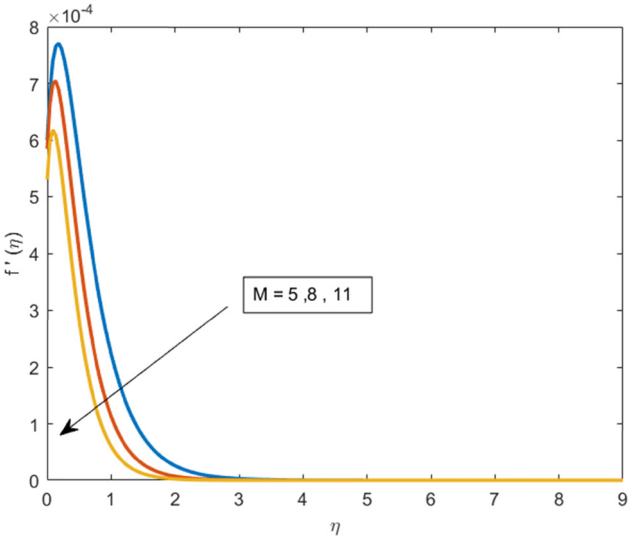

Figure 4: Velocity distribution for the magnetic parameter *M*.

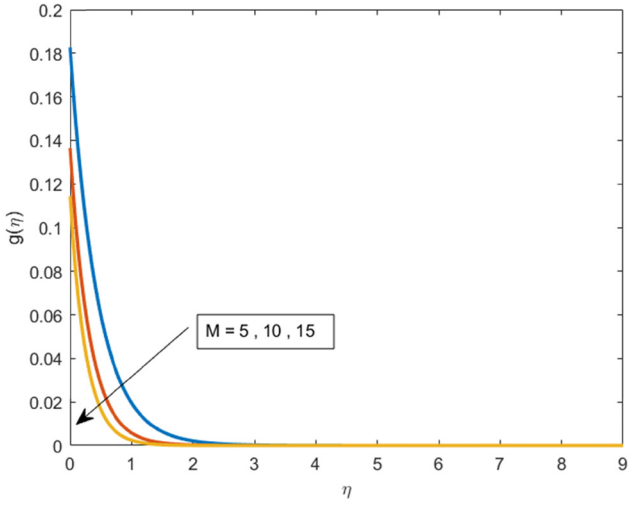

Figure 5: Velocity distribution for the magnetic parameter *M*.

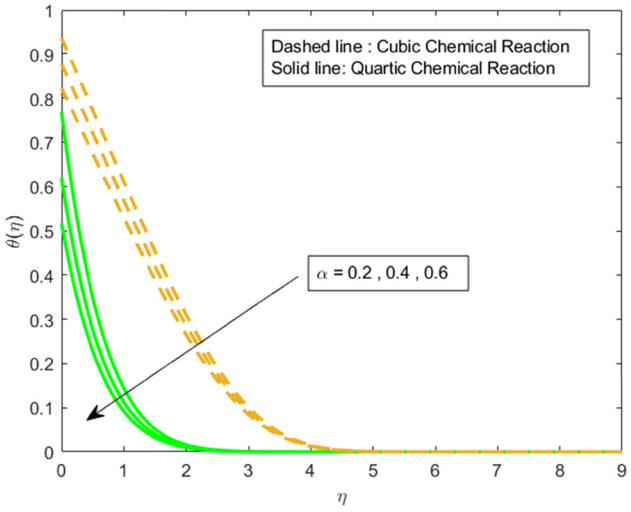

Figure 6: Temperature distribution parameter for the thermal slip parameter α.

parameter increases, this effect becomes more significant, resulting in a greater velocity across the flow profile.

The performance of the radial and axial velocities versus the magnetic parameter M is shown in Figures 4 and 5, respectively. It is witnessed that both profiles show a declining impact for the increased estimates of the magnetic factor. With the application of the magnetic field, the Lorentz force becomes stronger and shows resistance to the fluid flow. Eventually, a drop in both velocities is observed.

5.2 Temperature profile

Figures 6–9 show the temperature distribution $\theta(\eta)$ for the thermal slip parameter α, Brownian motion parameter N_b, thermophoresis parameter N_t, and the Prandtl number Pr.

The variation in the temperature profile $\theta(\eta)$ with an enhancement in the thermal slip parameter α is shown in Figure 6. A declining behavior is observed here. This is because the thermal jump condition affects the heat transfer at the boundary. In the case of a no-slip constraint, the temperatures of the liquid and surface are equal, and a maximum heat flux is observed. Nonetheless, in the case of a temperature jump condition, less heat is transmitted from the surface to the liquid, resulting in a reduction in the temperature profile. The temperature is decreased with enhancement in α for both cubic and quartic chemical reactions. The convergence of quartic chemical reactions is better than cubic chemical reactions.

The results of the Brownian motion parameter N_b versus the temperature profile are displayed in Figure 7. A drop in the temperature distribution is realized in this case. This occurs because the Brownian motion helps heat spread better through the fluid. As the Brownian motion increases, heat spreads more widely, leading to a more even temperature. Thus, the temperature profile becomes lower. Also, the quartic chemical reaction is stronger in this case.

Figure 8 illustrates the temperature profile for the thermophoresis parameter N_t. An increase in the temperature profile is observed for incremented estimates of the thermophoresis parameter. The thermophoresis effect drives the fluid particles from the hotter region to the colder one. Owing to this, a reduction in the heat transfer process is observed away from the hot area, resulting in

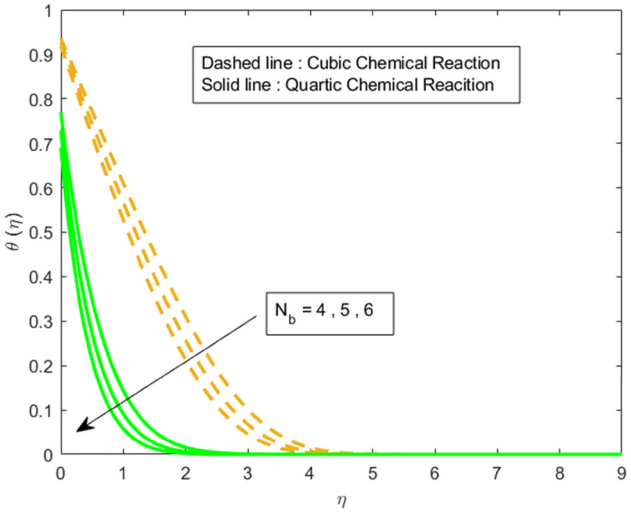

Figure 7: Temperature distribution for the Brownian motion parameter N_b.

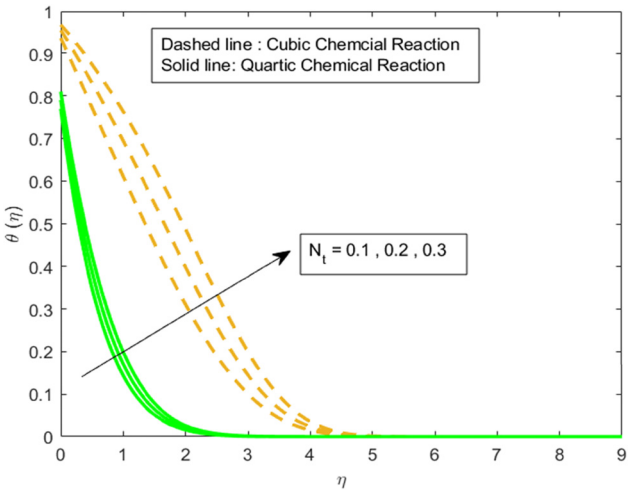

Figure 8: Temperature distribution for the thermophoresis parameter N_t.

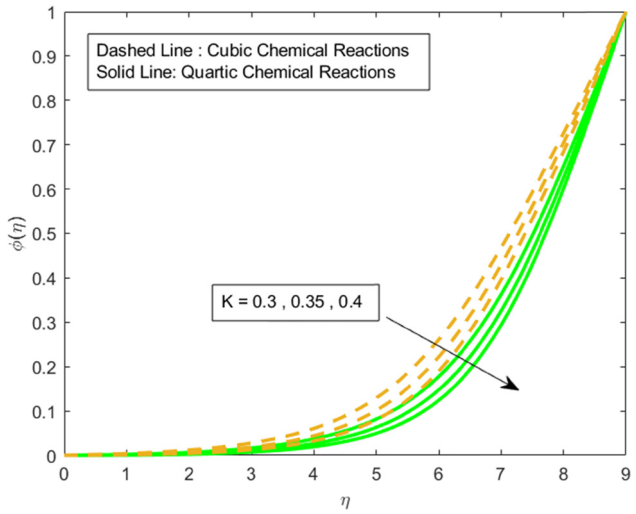

Figure 10: Concentration distribution for the Reiner–Rivlin parameter K.

the localized temperature. Thus, an increase in the overall temperature is observed, especially in the vicinity of the heat sources.

Figure 9 demonstrates a change in the temperature profile for the incremented values of the Prandtl number Pr. A decreasing behavior in the temperature profile is observed versus the Prandtl number. The Prandtl number is considered a quotient of momentum diffusivity to thermal diffusivity. Lower diffusivity will pave the path for the high Prandtl number, indicating that heat diffuses in the liquid more slowly, leading to a steeper temperature gradient and lower fluid temperature. Here, again, the effect of the quartic chemical reaction is stronger than the cubic chemical reaction.

5.3 Concentration profile

The impact of the Reiner–Rivlin parameter K on the concentration distribution is exhibited in Figure 10. A decline in the concentration distribution is observed here. The Reiner–Rivlin parameter portrays viscoelastic effects in the category of non-Newtonian liquids. With the increase in the Reiner–Rivlin parameter, the fluid resistance to deformation is enhanced, leading to stronger convective effects and reducing the local concentration. In response to the chemical processes, the graph shows consistent behavior with a declining trend in the parameter for both types of reactions. The outcomes for the cubic and quartic reactions are shown by the dashed and solid lines, respectively. The convergence of both lines is evident;

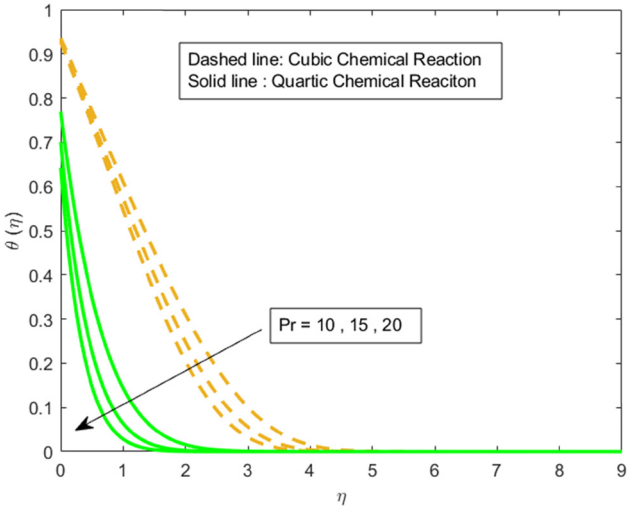

Figure 9: Temperature distribution for the Prandtl number Pr.

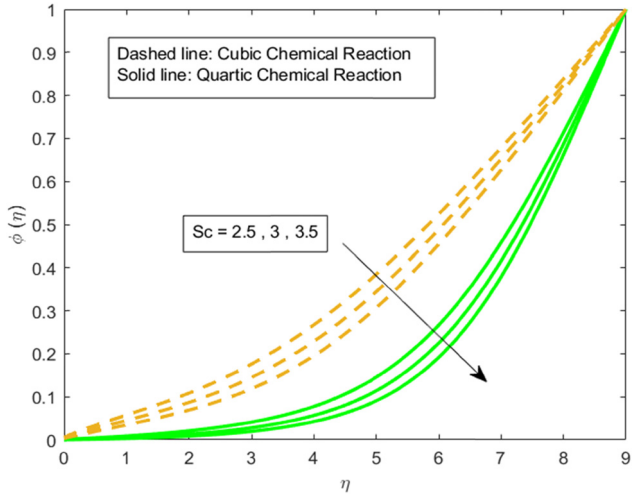

Figure 11: Concentration distribution for the Schmidt number Sc.

however, the quartic chemical reaction shows a stronger and more effective convergence than the cubic reaction. This implies that the quartic reaction attains stability in its behavior more successfully, emphasizing its greater impact on the dynamics of the system.

Figure 11 shows how the Schmidt number behaves versus the concentration profile, considering both quartic and cubic chemical processes. As the chemical processes proceed, the graph illustrates that the Schmidt number decreases for both kinds of reactions, indicating a drop in the fluid's mass and momentum diffusivity. The convergence of both lines indicates that, as a result of the chemical interactions, the system stabilizes over time. In contrast, the quartic chemical reaction exhibits a faster and more effective convergence than the cubic process. This enhanced convergence suggests that the diffusion processes are more favorably impacted by the quartic reaction, which results in a faster stabilization in the system.

6 Conclusions

In this study, the MHD Reiner–Rivlin nanoliquid flow over a rotating disk assisted by the partial slip and temperature jump conditions has been investigated. The novelty lies in considering a comparative analysis of the thermal performance of quartic and cubic chemical reactions. The numerical solution has been sought, and the results have been portrayed in the form of graphs and tables. The main findings of the current study are listed as follows:

- The velocity and temperature profiles exhibit opposing trends for the velocity and temperature slip parameters. This opposing trend arises due to the contrasting physical effects of the slip conditions on the momentum and thermal energy transfer.
- Both axial and radial velocity profiles display decreasing behaviors for the magnetic parameter. This damping is a well-known characteristic of MHD flows and plays a critical role in controlling the fluid motion in industrial applications like MHD pumps, cooling systems, and electromagnetic flow control.
- When a strong magnetic field is applied, more torque is necessary to maintain the disk's continuous spin. This principle is central to electromagnetic braking systems and is crucial in controlling MHD flows in turbines, plasma devices, and rotating machinery.
- Temperature distribution is diminishing against higher counts of the thermal slip factor, and this decreasing trend is more obvious for the quartic chemical reaction. This synergy between the thermal slip and strong reaction intensity explains the more obvious reduction in the temperature for quartic reactions.
- In the quartic chemical reaction case, the concentration distribution lowers significantly against high estimations of the Reiner–Rivlin parameter. This explains why the concentration profile diminishes more significantly in the quartic reaction scenario under strong non-Newtonian (Reiner–Rivlin) effects.
- The rate of heat flux is stronger in the case of a quartic chemical reaction than in a cubic chemical reaction. Here, the quartic reaction drives stronger thermal behavior, resulting in a higher rate of heat flux compared to the cubic chemical reaction.

7 Future scope

- Boger non-Newtonian nanofluid can be considered.
- Quadratic chemical reactions can be compared with cubic and quartic chemical reactions.
- Any other computational scheme may also be employed.

8 Limitations

- As the problem is highly nonlinear, it is very difficult to determine the exact solution.
- While the Reiner–Rivlin model captures certain non-Newtonian behaviors, it may not fully represent more complex rheological characteristics of real nanofluids.
- The model likely assumes uniform nanoparticle distribution, ignoring aggregation or sedimentation that can occur in real flows.

Acknowledgments: This work was supported and funded by the Deanship of Scientific Research at Imam Mohammad Ibn Saud Islamic University (IMSIU) (grant number IMSIU-DDRSP2503).

Funding information: This work was supported and funded by the Deanship of Scientific Research at Imam Mohammad Ibn Saud Islamic University (IMSIU) (grant number IMSIU-DDRSP2503).

Author contributions: Muhammad Ramzan: supervision and conceptualization. Yazeed Alkhrijah: formal analysis. Saeed Abbas: writing – original draft. Nazia Shahmir: software. Ibtehal Alazman: validation. Koh Wei Sin: writing –

review and editing. All authors have accepted responsibility for the entire content of this manuscript and approved its submission.

Conflict of interest: The authors state no conflict of interest.

Data availability statement: All data generated or analyzed during this study are included in this published article.

References

[1] Reiner M. A mathematical theory of dilatancy. Am J Math. 1945;67(3):350–62. doi: 10.2307/2371950.

[2] Rivlin RS. The hydrodynamics of non-Newtonian fluids. I. Proc R Soc Lond Ser A Math Phys Sci. 1948;193(1033):260–81. doi: 10.1098/rspa.1948.0044.

[3] Sabu AS, Mackolil J, Mahanthesh B, Mathew A. Reiner-Rivlin nanomaterial heat transfer over a rotating disk with distinct heat source and multiple slip effects. Appl Math Mech. 2021;42:42. doi: 10.1007/s10483-021-2772-7.

[4] Kumar S, Sharma K. Impacts of Stefan blowing on Reiner–Rivlin fluid flow over moving rotating disk with chemical reaction. Arab J Sci Eng. 2023;48(3):2737–46. doi: 10.1007/s13369-022-07008-9.

[5] Nebiyal A, Swaminathan R, Karpagavalli SG. Theoretical analysis of nanofluid's random diffusion with chemical reaction over a stretchable rotating disk using Homotopy Analysis Method. In AIP Conference Proceedings. Vol. 3160, No. 1, AIP Publishing; 2024. doi: 10.1063/5.0225247.

[6] Faisal M, Javed F, Badruddin IA, Ganie AH, Hussien M. Reiner Rivlin fluid flow between rotatable stretching disks with Cattaneo Christov heat transport. Numer Heat Transf Part A: Appl. 2024;1–20. doi: 10.1080/10407782.2024.2378182.

[7] Alarabi TH, Mahdy A, Abo-zaid OA. Distinctive approach for MHD natural bioconvection flow of Reiner–Rivlin nano-liquid due to an isothermal sphere. Case Stud Therm Eng. 2024;55:104179. doi: 10.1016/j.csite.2024.104179.

[8] Cham A, Mustafa M. Examining stagnation-point flow impinging on a deforming cylinder in Reiner-Rivlin fluid with integrated heat and mass transfer. Case Stud Therm Eng. 2024;20:104598. doi: 10.1016/j.csite.2024.104598.

[9] Muhammad T, Haider F. Time-dependent flow of Reiner–Rivlin nanofluid over a stretching sheet with Arrhenius activation energy and binary chemical reaction. Multidiscip Model Mater Struct. 2025;21(1):1–18. doi: 10.1108/MMMS-05-2024-0123.

[10] Li S, Naseer S, Shahmir N, Ramzan M, Alkarni S, Kadry S. Influence of magnetic dipole and thermophoretic particle deposition on the flow of Reiner–Philippoff fluid with Thompson and Troian slip. ZAMM-J Appl Math Mech/Zeitschrift für Angewandte Mathematik und Mechanik. 2025;105(2):e202400098. doi: 10.1002/zamm.202400098.

[11] Gangadhar K, Sree TS, Wakif A, Subbarao K. Stefan blowing impact and chemical response of Rivlin–Reiner fluid through rotating convective disk. Pramana. 2024;98(4):160. doi: 10.1007/s12043-024-02836-w.

[12] Abhijith P, Areekara S, Sabu AS, Mathew A. MHD Reiner-Rivlin nanofluid flow considering Soret-Dufour and nonlinear chemical reaction. Multiscale Multidiscip Model Exp Des. 2025;8(1):33. doi: 10.1007/s41939-024-00616-y.

[13] Ramzan M, Riasat S, Kadry S, Chu YM, Ghazwani HAS, Alzahrani AK. Influence of autocatalytic chemical reaction with heterogeneous catalysis in the flow of Ostwald-de-Waele nanofluid past a rotating disk with variable thickness in porous media. Int Commun Heat Mass Transf. 2021;128:105653. doi: 10.1016/j.icheatmasstransfer.2021.105653.

[14] ur Rahman M, Haq F, Ghazwani HA, Khan MI, Abduvalieva D, Ali S, et al. Darcy-Forchheimer flow of Prandtl nanofluid with irreversibility analysis and cubic autocatalytic chemical reactions. Bio Nanosci. 2023;13(4):1976–87. doi: 10.1007/s12668-023-01212-z.

[15] Xin X, Jamshed W, Eid MR, Safdar R, Hussain SM, Ahmad H, et al. Numerical case study of cubic autocatalysis nanotechnology of slanted magnetic force and slippage velocity of three-dimensional Carreau nanofluid flow. Bio Nanosci. 2024;14(2):1–16. doi: 10.1007/s12668-024-01343-x.

[16] Khan MP, Chang CY, Raja MAZ, Shoaib M. Intelligent adaptive nonlinear autoregressive eXogeneous neuro-structure for ferromagnetic Powell -Eyring fluidic involving cubic autocatalysis chemical reaction. ZAMM-J Appl Math Mech/Zeitschrift für Angewandte Mathematik und Mechanik. 2025;105(1):e202300748. doi: 10.1002/zamm.202300748.

[17] Atif SM, Khan WA, Abbas M, Rashid U. Bioconvection mangneto hydrodynamic tangent hyperbolic nanofluid flow with quartic chemical reaction past a paraboloid surface. Comput Model Eng Sci. 2022;130(1):205–20. doi: 10.32604/cmes.2022.017304.

[18] Saranya S, Ragupathi P, Al-Mdallal QM, Said S. A study of effects of H– H quartic auto-catalytic reaction with equal diffusivity in the swirling flow exterior to a rotating cylinder. Int J Thermofluids. 2023;20:100441. doi: 10.1016/j.ijft.2023.100441.

[19] Oreyeni T, Obalalu AM, Popoola AO, Omole EO, Souayeh B, Ajewole KP, et al. Quartic autocatalytic reaction in a bioconvective flow of a stratified EHMD Casson fluid conveying nanoparticles over a surface with variable thickness: Legendre based collocation approach. In 2024 International Conference on Science, Engineering and Business for Driving Sustainable Development Goals(SEB4SDG). IEEE; 2024. p. 1–14. doi: 10.1109/SEB4SDG60871.2024.10629791.

[20] Riaz M, Khan N, Hashmi MS, Tawfiq FM, Bilal M, Inc M. Analysis of Darcy–Forchheimer flow of magnetized hybrid nanofluid (MoS_2 + ZnO/E) with non-linear heat source and quartic autocatalytic chemical reaction. Numer Heat Transf Part A: Appl. 2024;1–21. doi: 10.1080/10407782.2024.2383844.

[21] Mehmood Y, Alsinai A, Niazi AUK, Bilal M, Akhtar T. Numerical study of Maxwell nanofluid flow with MWCNT and SWCNT considering quartic autocatalytic reactions and Thompson-Troian slip mechanism. Discov Appl Sci. 2024;6(10):534. doi: 10.1007/s42452-024-06243-z.

[22] Gangadhar K, Naga Chandrika G, Dinarvand S. Simulation of radiative nonlinear heat dynamism on Buongiorno-modeled nanoliquid through porous inclined plate with adjustable chemical response. Mod Phys Lett B. 2024;38(34):2450347. doi: 10.1142/S0217984924503470.

[23] Hayat T, Bashir A, Khan SA, Alsaedi A. Reiner-Rivlin nanofluid over a rotating disk flow. Chem Phys Lett. 2022;797:139556. doi: 10.1016/j.cplett.2022.139556.

[24] Yu B, Ramzan M, Riasat S, Kadry S, Chu YM, Malik MY. Impact of autocatalytic chemical reaction in an Ostwald-de-Waele nanofluid flow past a rotating disk with heterogeneous catalysis. Sci Rep. 2021;11(1):15526. doi: 10.1038/s41598-021-94918-7.
[25] Mustafa M. MHD nanofluid flow over a rotating disk with partial slip effects: Buongiorno model. Int Commun Heat Mass Transf. 2017;108:1910–6. doi: 10.1016/j.ijheatmasstransfer.2017.01.064.
[26] Chaudhary MA, Merkin JH. A simple isothermal model for homogeneous- heterogeneous reactions in boundary-layer flow. I Equal diffusivities. Fluid Dyn Res. 1995;16(6):311–33. doi: 10.1016/0169-5983(95)00015-6.
[27] Ouyang Y, Md Basir MF, Naganthran K, Pop I. Stability analysis of unsteady ternary nanofluid flow past a stretching/shrinking wedge. Open Phys. 2025;23(1):20250148. doi: 10.1515/phys-2025-0148.
[28] Galal AM, Saadeh R, Obalalu AM, Khan U, Elattar S. Dissipative disorder optimization in the radiative thin film flow of partially ionized non-Newtonian hybrid nanofluid with second-order slip condition. Open Phys. 2025;23(1):20250149. doi: 10.1515/phys-2025-0149.
[29] Hai T, Basem A, Alizadeh AA, Singh PK, Rajab H, Maatki C, et al. Optimizing ternary hybrid nanofluids using neural networks, gene expression programming, and multi-objective particle swarm optimization: a computational intelligence strategy. Sci Rep. 2025;15(1):1986. doi: 10.1038/s41598-025-85236-3.
[30] Tabassum M, Mustafa M. A numerical treatment for partial slip flow and heat transfer of non-Newtonian Reiner-Rivlin fluid due to rotating disk. Int J Heat Mass Transf. 2018;123:979–87. doi: 10.1016/j.ijheatmasstransfer.2018.03.040.

Appendix

The derivatives used to convert PDEs into ODEs are as follows:

$$\frac{\partial u}{\partial r} = \Omega f'(\eta), \quad \frac{u}{r} = \Omega f'(\eta), \quad \frac{\partial w}{\partial z} = -2\Omega f'(\eta)$$

$$\begin{aligned}
&\frac{\partial u}{\partial r} = \Omega f'(\eta), \frac{v}{r} = \Omega g(\eta), \frac{\partial v}{\partial r} = \Omega g(\eta), \frac{\partial w}{\partial r} = 0,\\
&\frac{\partial u}{\partial z} = r\Omega\sqrt{\frac{\Omega}{\upsilon_f}} f''(\eta), \frac{\partial w}{\partial r} = 0, \frac{\partial T}{\partial r} = 0,\\
&\frac{\partial T}{\partial z} = \theta'(\eta)(T_w - T_\infty)\sqrt{\frac{\Omega}{\upsilon_f}}, \quad \frac{\partial^2 T}{\partial r^2} = 0,\\
&\frac{\partial^2 T}{\partial z^2} = \theta''(\eta)(T_w - T_\infty)\frac{\Omega}{\upsilon_f}, \quad \frac{\partial a}{\partial r} = 0, \frac{\partial a}{\partial z} = a_\infty {\phi_1}'(\eta)\sqrt{\frac{\Omega}{\upsilon_f}},\\
&\frac{\partial b}{\partial r} = 0, \quad \frac{\partial b}{\partial z} = a_\infty {\phi_2}'(\eta)\sqrt{\frac{\Omega}{\upsilon_f}},\\
&\frac{\partial T}{\partial z} = \theta'(\eta)(T_w - T_\infty)\sqrt{\frac{\Omega}{\upsilon_f}}, \quad \frac{\partial^2 T}{\partial z^2} = \theta''(\eta)(T_w - T_\infty)\frac{\Omega}{\upsilon_f},\\
&\frac{\partial a}{\partial r} = 0, \quad \frac{\partial a}{\partial z} = a_\infty {\phi_1}'(\eta)\sqrt{\frac{\Omega}{\upsilon_f}},\\
&\frac{\partial^2 a}{\partial z^2} = a_\infty {\phi_1}''(\eta)\frac{\Omega}{\upsilon_f}, \quad a = a_\infty \phi_1(\eta), \quad b = a_\infty \phi_2(\eta),\\
&\frac{\partial T}{\partial z} = \theta'(\eta)(T_w - T_\infty)\sqrt{\frac{\Omega}{\upsilon_f}}, \quad \frac{\partial^2 T}{\partial z^2} = \theta''(\eta)(T_w - T_\infty)\frac{\Omega}{\upsilon_f},\\
&\frac{\partial b}{\partial r} = 0, \quad \frac{\partial b}{\partial z} = a_\infty {\phi_2}'(\eta)\sqrt{\frac{\Omega}{\upsilon_f}},\\
&\frac{\partial^2 b}{\partial z^2} = a_\infty {\phi_2}''(\eta)\frac{\Omega}{\upsilon_f}, \quad b = a_\infty \phi_2(\eta).
\end{aligned} \tag{A1}$$